

Article

Ultrafast Fiber Laser Emitting at 2.8 μm Based on a SESAM and a Broadband FBG

Pascal Paradis , Tommy Boilard , Vincent Fortin, Réal Vallée and Martin Bernier

Center for Optics, Photonics and Lasers, Université Laval, Quebec, QC G1V 0A6, Canada; tommy.boilard.1@ulaval.ca (T.B.); vincent.fortin@copl.ulaval.ca (V.F.); rvallee@copl.ulaval.ca (R.V.); martin.bernier@copl.ulaval.ca (M.B.)

* Correspondence: pascal.paradis.2@ulaval.ca

Abstract: Ultrafast mid-infrared fiber lasers have been intensely studied in the last decade for the generation of high harmonics, molecular spectroscopy, material processing and remote sensing. Different designs have been investigated but most of them lacked the ease of use and reliability needed for their democratization. In this paper, we demonstrate a self-starting mode-locked mid-IR erbium-doped fiber laser based on a SESAM and a broadband uniform FBG that produces pulses as short as 15 ps. Different laser cavities were tested with varying FBG peak reflectance, spectral bandwidth and active fiber length. In addition, one cavity uses a pump combiner instead of injecting free-space the pump power through the fiber tip. The results of this study confirm that the FBG spectral bandwidth can efficiently control the duration of the almost Fourier-transform-limited pulses up to a limit seemingly dictated by the presence of water vapor in the laser cavity acting as narrow spectral filters. To a lower effect, the active fiber length influences the pulse duration. Finally, the use of an all-fiber pump combiner allows for a more compact and rugged design without altering the laser performances. This study represents a step towards the development of robust mid-infrared ultrafast all-fiber lasers.

Keywords: mid-infrared; fiber lasers; pulsed lasers; mode-locking; ultrafast lasers



Citation: Paradis, P.; Boilard, T.; Fortin, V.; Vallée, R.; Bernier, M. Ultrafast Fiber Laser Emitting at 2.8 μm Based on a SESAM and a Broadband FBG. *Photonics* **2023**, *10*, 753. <https://doi.org/10.3390/photronics10070753>

Received: 21 April 2023

Revised: 16 June 2023

Accepted: 27 June 2023

Published: 29 June 2023



Copyright: © 2023 by the authors. Licensee MDPI, Basel, Switzerland. This article is an open access article distributed under the terms and conditions of the Creative Commons Attribution (CC BY) license (<https://creativecommons.org/licenses/by/4.0/>).

1. Introduction

In the last decade, there has been a lot of research on ultrafast mid-infrared (mid-IR) lasers due to their ability to generate high harmonics and to perform applications in molecular spectroscopy, material processing and remote sensing. Such lasers are especially interesting for their single mode beam profile as well as their overall performances and efficiency [1–3] compared to solid-state lasers including optical parametric oscillators and amplifiers (OPO and OPA). Ultrafast fiber lasers operating in picosecond regime at 2.8 μm are envisioned for efficient laser processing of biomedical materials since they can benefit from the large peak absorption of water near 2.9 μm [4–6]. Such mid-IR ultrafast laser sources can also be very useful for the generation of supercontinuum at longer wavelengths in the mid-infrared that find numerous applications in spectroscopy and remote sensing [7,8]. Accordingly, many promising applications are currently under development and are calling from such sources, namely living cell printing [9], laser-based mass spectrometry of diseases [10], laser breath analyzing [11], etc.

Different mode-locking techniques for mid-IR fiber lasers have been investigated during the last decade [3]. The first femtosecond mode-locked fiber lasers operating at mid-IR wavelengths was demonstrated in 2015 [12,13]. Those two laser systems were designed as ring cavities using the non-linear polarization evolution inside the fiber combined to a polarization-dependent isolator as saturable absorption mechanism to achieve mode locking. Further optimization of this design led to peak powers up to tens of kilowatts and pulses with duration around 200 fs generated directly from the laser cavity around 2.8 μm [14,15]. Ultrafast ring fiber lasers were also demonstrated at longer wavelengths,

namely at 3.2 μm and 3.5 μm [16,17]. In recent years, pulses of just a few tens of femtoseconds with peak powers reaching the megawatt level at a wavelength around 2.8 μm were reported with chirped pulse amplification of pulses from ring cavities [18,19]. A simpler design with a semiconductor saturable absorber mirror (SESAM), non-linear mirrors and two-dimensional materials have been used to achieve picosecond mode-locked fiber lasers emitting around 2.8 μm [20–28], and even up to 3.5 μm [29,30]. In reference [31], the use of a chirped FBG in combination with a SESAM reported stable mode-locking of a linear cavity producing relatively long pulses of 60 ps duration. Recently, a mode-locked all-fiber laser has even been demonstrated with a black phosphorus layer deposited directly onto the active fiber tip [32] and another one was demonstrated with a home-made MXene saturable absorber butt-coupled to the gain fiber [33]. However, those demonstrations were made with home-made saturable absorbers that are efficient enough when butt-coupled to the fiber tip as compared to the suboptimal but more easily available commercial solutions. Also, the issue of their reliability was not really investigated. Moreover, the effect of the design of those laser systems were not fully characterized since the pulse duration and chirp were not measured due to the lack of suitable instruments in many of the aforementioned demonstrations.

In this manuscript, we proceed to a thorough investigation of a mode-locked fiber laser emitting pulses as short as 15 ps at 2.8 μm based on a SESAM and a broadband uniform fiber Bragg grating (FBG). We namely report on the impact of the fiber length, the FBG peak reflectance and spectral bandwidth upon producing optimized pulses. We perform a complete pulse characterization including a frequency resolved optical gating (FROG) measurement. We show that the duration of the almost Fourier-transform-limited pulses can be efficiently controlled by the FBG spectral bandwidth up to a limit which is likely dictated by the presence of water vapor in the laser cavity acting as narrow spectral filters, but could also be due to the SESAM used as saturable absorber. This study represents a step towards the development of robust all-fiber ultrafast mid-infrared fiber lasers.

2. Materials and Methods

We used 4 different laser cavities to verify the effect of the FBG peak reflectance and bandwidth on the mode-locked pulses duration. The parameters of each laser cavity are summarized in Table 1. The experimental setup shown in Figure 1 is the same for the laser cavities 1, 2 and 3, whereas Figure 2 shows the fourth laser cavity setup which includes a pump combiner. The four laser cavities share several common components and features. A multimode laser diode (AM6-976B-10-604, *Alfalight*, Madison, WI, USA) emitting a maximum power of 7 W centered at 976 nm is used as the pump source. The active fiber is a 7 mol.% erbium-doped fluoride fiber from *Le Verre Fluoré* (Bruz, France) with a core diameter of 16 μm and a cladding diameter of $240 \times 260 \mu\text{m}$ (double-D shape). All the fiber tips are angle-cleaved at about 6° to avoid parasitic feedback in the laser cavity. One side of the laser cavities is bounded by a SESAM (SAM-3000-33-10 ps, *BATOP GmbH*, Jena, Germany) with a modulation depth of 18%, non-saturable losses of 15%, a saturation fluence of 70 $\mu\text{J}/\text{cm}^2$ and a relaxation time of 10 ps. The cavity output end is bounded by a FBG that was written with femtosecond pulses directly through the protective coating of the fiber with a phase-mask technique to preserve the robustness of the fiber [34]. To control the bandwidth of the FBG while minimizing its chirp, we used a uniform FBG of variable but short length, recalling that the shorter its length, the wider its reflectance bandwidth. All the ZnSe lenses have an antireflective coating to avoid parasitic feedback and to reduce the intracavity losses as much as possible. However, as presented in Table 1, the FBG peak reflectance, central wavelength and bandwidth are specific to each laser cavity. The active fiber length is also unique to each setup.

All the measurements were made with a germanium filter (WG91050-C9, *Thorlabs*, Newton, MA, USA) at the laser output to remove any residual pump or fluorescence signals below 1.9 μm . The average power of the laser is measured with a thermopile (XLP12-3S-H2-D0, *Gentec-EO*, Quebec, QC, Canada) and the optical spectra are measured with an optical

spectrum analyzer (AQ6376, *Yokogawa*, Tokyo, Japan). The pulse trains are obtained with a MCT photodiode (KV104, *Kolmar*, Zug, Switzerland) having a bandwidth of 1 GHz, and a photodiode with a rise time of 200 ps (UPD-5N-IR-2P, *Alphalas*, Göttingen, Germany), both acquired with a 500 MHz oscilloscope (GDS-3504, *GwInstek*, New Taipei City, Taiwan). The RF spectra are measured with an RF spectrum analyzer (RSA 3303A, *Tektronix*, Beaverton, OR, USA). Finally, an autocorrelator (FR-103X, *Femtochrome*, Berkeley, CA, USA) and a second-harmonic frequency-resolved optical gating (FROG) instrument (custom designed, *Few-Cycle*, Montreal, QC, Canada) were used to measure the pulse duration and chirp.

Table 1. Parameters of the laser cavities.

Laser Cavity	FBG Reflectance (%)	FBG Bandwidth (nm)	FBG Central Wavelength (nm)	Fiber Length (m)
1	82–35	0.7	2791.0	2
2	65	3.2	2790.9	2
3	23	7.2	2792.5	4–1.25
4	58	6.8	2793.1	2

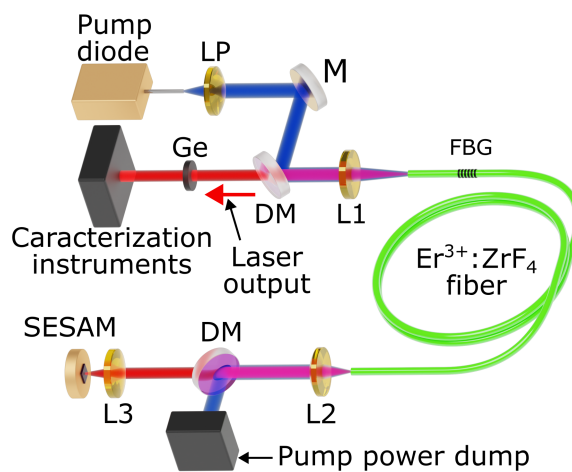


Figure 1. Experimental setup used with laser cavities 1, 2 and 3 to test the performances of the laser based on the FBG bandwidth and peak reflectance (LP: CaF₂ lens, $f = 11$ mm; M: gold mirror; DM: dichroic mirror; Ge: germanium filter; L1: ZnSe lens, $f = 25$ mm; L2 and L3: ZnSe lens, $f = 12.5$ mm).

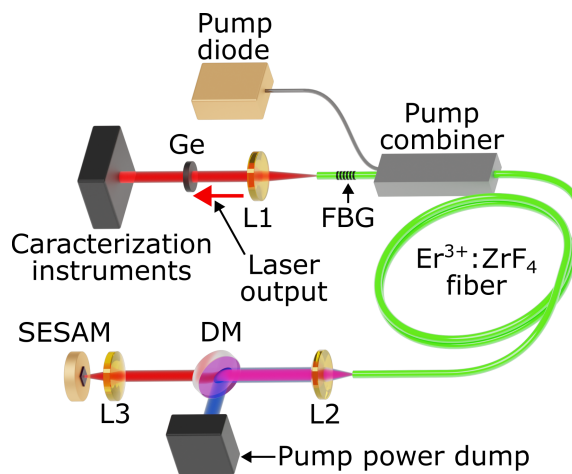


Figure 2. Experimental setup of the mode-locked fiber laser 4 with a pump combiner (DM: dichroic mirror; Ge: germanium filter; L1: ZnSe lens, $f = 25$ mm; L2 and L3: ZnSe lens, $f = 12.5$ mm).

The FBG parameters were investigated first. The FBG peak reflectance was optimized with the laser cavity 1. For this first laser cavity, we wrote a FBG with a peak reflectance of

82% centered at 2791.0 nm and a spectral width of 0.7 nm. It was heated at 70 °C for 5 min to stabilize it enough for the experiment without fixing it completely. To be able to compare the laser behavior based on the FBG peak reflectance, we kept the same laser cavity and alignment but proceeded to a thermal treatment of the FBG at different temperatures (90 °C, 110 °C, 130 °C, 150 °C) for 5 min to lower its refractive index modulation and thus its peak reflectance. A separate FBG with similar parameters was studied in parallel and showed that each annealing step reduced further its peak reflectance as follows: 70%, 58%, 47%, 35%. The FBG bandwidth is the second parameter that we studied with two other FBGs: the one in the laser cavity 2 with a bandwidth of 3.2 nm centered at 2790.9 nm and a peak reflectance of 65% and another one in the laser cavity 3 with a bandwidth of 7.2 nm centered at 2792.5 nm and a peak reflectance of 20%. The maximum peak reflectance that we could achieve was limited because the FBGs were written as short as possible to obtain the largest possible bandwidth. Then, we verified the effect of the active fiber length on the pulse duration with the laser cavity 3. This laser cavity started with a 4 m-long fiber that we shortened subsequently to 3 m, 2.5 m, 2.1 m, 1.75 m, 1.5 m and 1.25 m. The fourth laser cavity was made with a pump combiner and an FBG with a bandwidth of 6.8 nm and a peak reflectance of 58%. All the free space optical components related to the pump injection into the gain fiber, i.e., the pump lens (LP), a gold mirror (M) and the dichroic mirror at the output of the laser cavity (DM), were replaced in this design by the all-fiber pump combiner.

3. Results

The FBG transmission spectra and the laser emission spectra corresponding to the shortest pulses generated by the laser cavities are presented in Figure 3. These are also compared to the transmission spectrum of the atmospheric water vapor to better understand the limitation caused by the free-space propagation within the laser cavities. The best emission spectrum from the laser 1 with a FBG peak reflectance of 70% has a FWHM of 0.22 nm. The laser emission spectrum generated by the laser 2 has a FWHM of 0.65 nm. The laser 3 with a fiber length of 1.25 m produced a laser bandwidth at FWHM of 0.33 nm. And the laser-4 generated a laser emission spectrum as large as 0.42 nm at FWHM. The signal-to-noise ratio of the spectrum of the third laser cavity is much lower than the other cavities due to the lower average power of that specific measurement. The laser output spectra are all centered on their respective FBG reflectance spectrum. The specific central wavelength and bandwidth of the FBGs spectra combined with the water vapor absorption spectrum can explain the limited laser bandwidth and pulse duration even though they are all centered around 2792 ± 2 nm [35]. The laser emission bandwidths appear to be either limited by the FBG bandwidth or the water vapor absorption peaks around 2.8 μ m. Fiber lasers generating strong mode-locked soliton pulses based on the nonlinear polarization evolution can overcome the bandwidth limitation of the water vapor absorption peaks. However, our fiber lasers using a finite response time saturable absorber could not produce pulses with high enough peak power that could lead to the sufficient nonlinear phase accumulation to sustain a soliton regime, similarly to what was reported by Majewski et al. [35]. Interestingly though, the emission spectrum of laser 4 overlaps slightly with the strong water absorption line on the shorter wavelength side. Our hypothesis on this behavior is that the laser bandwidth might be limited by the free-space propagation inside the laser cavity, but the spectrum could be broadened when the signal propagates in the gain fiber towards the output of the laser system. Another hypothesis for the limitation of the laser bandwidth could be the SESAM's parameters such as its recovery time and its dispersion which we were not able to measure. All of the laser cavities operated in a self-starting continuous-wave (CW) mode-locked regime without passing through a Q-switching regime at lower pump power when the alignment was optimized for the CW mode-locked regime.

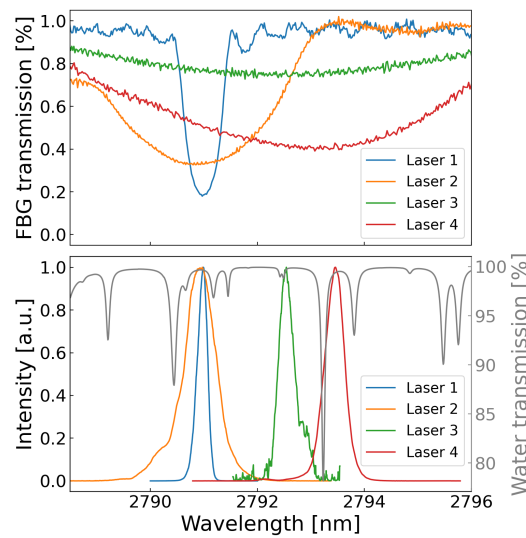


Figure 3. FBG transmissions (**top**) along with the corresponding emission spectrum from each laser cavity (**bottom**), superimposed to the transmission spectrum of the atmospheric water vapor for 40 cm of propagation in air based on a Hitran simulation (in gray). The specific parameters of each laser cavity are detailed in Table 1. More particularly, laser 1 has a FBG peak reflectance of 70% and laser 3 has a fiber length of 1.25 m.

3.1. FBG Peak Reflectance

To assess the effect of the FBG peak reflectance while keeping the same laser cavity and alignment, the FBG of cavity 1 is heated at different temperatures for 5 min at a time at increasing temperature steps of 90 °C, 110 °C, 130 °C and 150 °C. By doing so, the peak reflectance is lowered by about 10% each time. The initial heating temperature of the FBG was 70 °C to obtain the reflectance of 82%. and each additional annealing step reduced further its reflectance to about 70%, 58%, 47% and 35%. For each reflectance, the pulse train, the output spectrum and an autocorrelation trace were measured. Figure 4 shows the pulse duration and average power of the mode-locked laser as a function of the FBG reflectance. One can observe that the average power increases with the lower FBG peak reflectance as expected, while the bandwidth of the pulses is at its widest when the pulses are the shortest. The difference between the values of bandwidth at the two lowest reflectances is within the resolution limit of the OSA. The shortest pulses are generated at a fairly high peak reflectance around 70%. High intra-cavity losses caused by the lenses, the dichroic mirror, the SESAM and the reinjection of the signal into the fiber could explain the need for a high output coupler reflectance to counter all these losses. However, the higher reflectance of the FBG also lowers the output power of the laser, thus lowering the lasing efficiency. The performance of this laser cavity is also consistent with a previous demonstration using similar parameters [31].

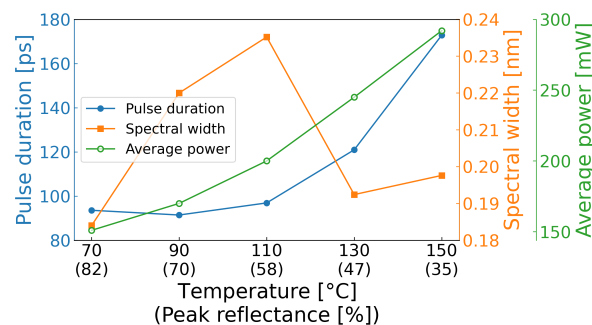


Figure 4. Pulse duration, spectral width and average power depending on the FBG peak reflectance (heating temperature) for cavity 1.

3.2. The FBG Bandwidth

As we wanted to generate much shorter pulses, we also studied the effect of the FBG bandwidth using a new laser cavity based on the same setup as in Figure 1 and the same fiber length, but using a FBG with a peak reflectance of 65% centered at 2790.9 nm and a bandwidth of 3.2 nm [36]. Those FBG parameters lead to the shortest pulses from a mode-locked fiber laser based on a SESAM and an FBG operating at 2.8 μm . This particular laser cavity (cavity 2) generates 15 ps pulses with an average power of 150 mW at a repetition rate of 55 MHz. Figure 5 shows the emission spectrum and the autocorrelation trace of the shortest pulses generated by this laser cavity. The time-bandwidth product based on these is 0.380, i.e., close to the Fourier-transform limit. The FROG trace and the retrieved pulse shape are also consistent with this observation (cf. Figure 6). The sech^2 fit in Figure 5 shows an optimal pulse duration of 12 ps based on the pulse bandwidth instead of the 15 ps as measured with the autocorrelator. These pulses are mostly unchirped because the dispersion length L_D of this fiber is 950 m for these pulses, which is much longer than the round-trip distance of any of the laser cavities that were tested thus confirming that the dispersion is not significant. The non-linear length L_{NL} in this case is 33 m, which is much shorter than the dispersion length, but still significantly longer than the cavity length. We believe that the residual dispersion leading to this time–bandwidth product could arise from the water absorption peaks surrounding the pulse spectrum or from the free space components, especially the SESAM. The mode-locked pulse train is stable with a signal-to-noise ratio around 70 dB as shown in Figure 7. Since this FBG and that of cavity 1 with a bandwidth of 0.7 nm are both centered around the 2791 nm transmission window, the only significant difference between the two laser cavities is the FBGs bandwidth. This points to the FBG bandwidth as being an important limiting factor for further shortening the pulse duration, as expected.

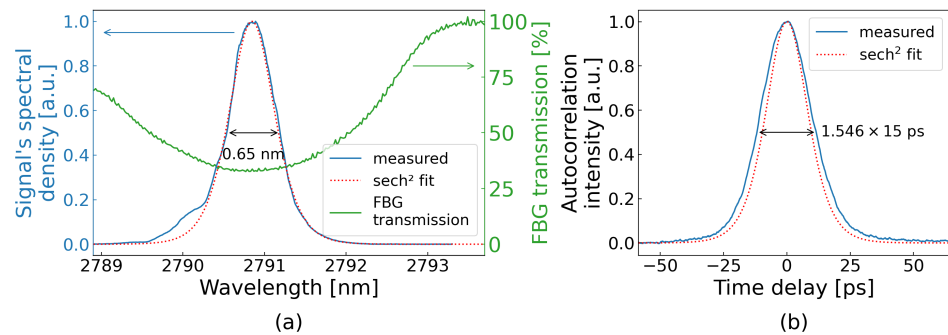


Figure 5. (a) Laser emission spectrum and its sech^2 fit along with the FBG transmission spectrum. (b) Autocorrelation trace of the mode-locked pulses generated by the laser cavity 2.

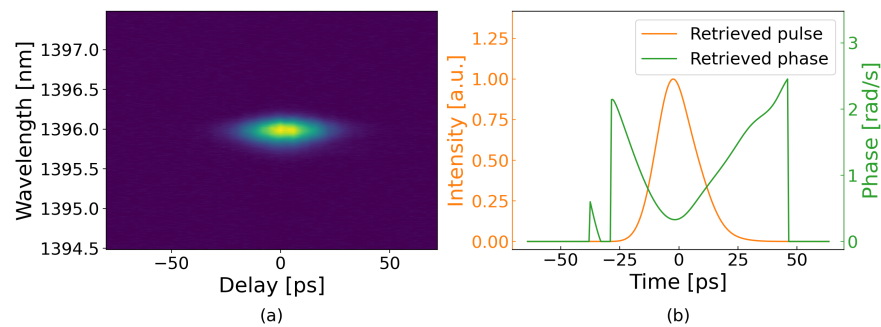


Figure 6. (a) FROG trace and (b) the corresponding retrieved pulse shape and phase of the 15 ps pulses generated by the laser cavity 2.

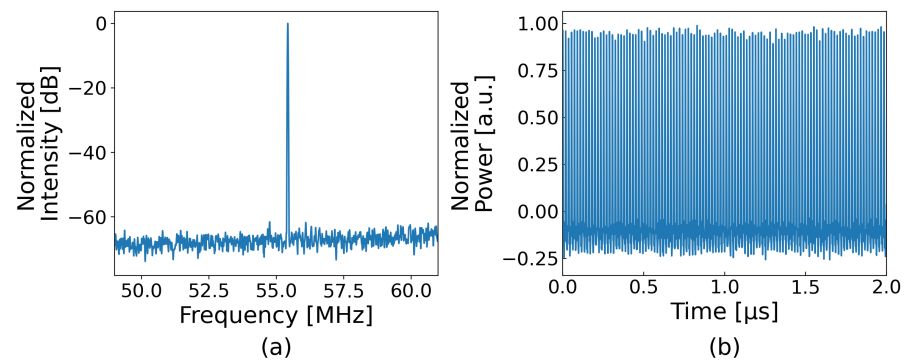


Figure 7. (a) RF signal of the 15 ps-long pulses emitted by the cavity 2 and (b) its corresponding pulse train.

However, the pulses emitted by the laser cavity 3 having a broader FBG with a peak reflectance of 20% were not shorter than those of the second laser cavity despite also being almost Fourier-transform limited. The 1.25 m-long laser cavity 3 could only generate pulses as short as 23 ps as measured with the FROG instrument as shown in Figure 8. Moreover, the pulses were less stable. The instability and narrower bandwidth might be explained by the interaction of the laser spectrum with one of the water absorption lines in the free-space portion of the laser cavity [35] (see Figure 3). Unfortunately, it was not possible to butt-couple the SESAM to the gain fiber to avoid the free-space propagation and thus to remove the bandwidth limitation caused by the water vapor because the specific mid-IR SESAM used in this demonstration has a reverse design. In this SESAM design, the laser beam goes through the antireflective coating, the saturable absorber layer, which is GaAs wafer with a thickness of 625 μm, and the substrate layer before finally being reflected back by a gold mirror. Butt-coupling the SESAM at the output gain fiber would therefore have resulted in significant recoupling losses. Another possible explanation for the bandwidth limitation of the laser pulses could be that the SESAM could not support shorter pulses due to its parameters but we were not able to verify those experimentally.

3.3. Laser Cavity Length Effect

As evidenced by the results of the third laser cavity shown in Figure 8, a shorter laser cavity favors shorter pulses as reported in other demonstrations in the near-infrared and mid-infrared wavelengths [14,37,38]. This might be due to the reduced dispersion and non-linear effects in the laser cavity according to those previous demonstrations. Another hypothesis to explain this behavior is that the reduced gain inside the laser cavity might also favor the shorter pulse duration because the background noise is less amplified. The laser cavity with 1.25 m of erbium-doped fluoride fiber produced pulses with a duration of 23 ps as measured with the FROG instrument. However, it seems that for laser cavities longer than 1.75 m, the pulse duration is stable around 55 ps. Since the different lengths were obtained by cleaving the active fiber at the fiber end adjacent to the free-space propagation path of the laser cavity, the alignment of the beam inside the cavity had to be optimized every time and that could explain the large fluctuation of spectral bandwidth and average power as a function of fiber length. Still, the trend with respect to pulse duration seemed more consistent.

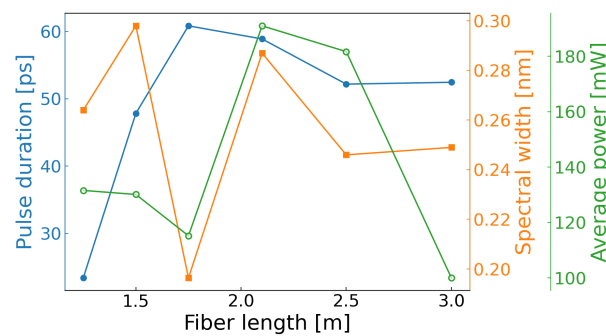


Figure 8. Pulse duration, spectral width and average power depending on the length of the cavity 3.

3.4. Pump Combiner Effect

To achieve a mode-locked all-fiber laser design based on a SESAM, the use of a pump combiner is crucial for the injection of the pump power into the laser cavity without free-space propagation and to free the output end of the fiber as illustrated in Figure 2. This laser cavity 4 produces pulses as short as 21 ps as calculated from the FROG trace in Figure 9. Thus, the pulse duration is close to the Fourier-transform limit with a time–bandwidth product of 0.357. So, the use of a pump combiner inside the laser cavity is not problematic to ensure a stable mode-locking with the clear advantage of an all-fiber pump injection configuration. The slightly longer pulse duration might just be caused by the specific transmission window the central wavelength of the laser is in as shown in Figure 3.

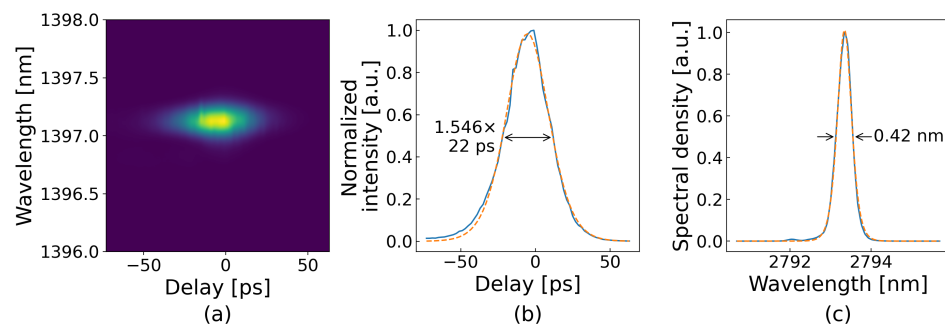


Figure 9. (a) FROG trace, (b) autocorrelation trace and (c) emission spectrum of the shortest pulses produced by the laser cavity 4.

4. Discussion

We first showed that the pulsed duration can be minimized with an optimized output coupler peak reflectance. With this design, a low output reflectance increases the average output power, thus the pulse energy, but the pulse duration is also increased, probably because the pulse peak power inside the laser cavity is lower. We also showed that the pulse duration is shortened with a shorter laser cavity just like what has been reported for near-IR and mid-IR mode-locked fiber lasers. However, a shortened laser cavity also increases the fundamental repetition rate of the pulses and its effect on the pulse duration is limited by the actual possible bandwidth of the laser emission. So, the fiber length might not be the best parameter to adjust to obtain the desired pulse duration. In this design, the FBG reflectance spectrum has the biggest impact on the pulse duration. Their duration can be adjusted by using an FBG with a narrower or broader reflectance spectrum since the mode-locked pulses are close to being Fourier-transform limited. However, the laser emission spectrum could not be broadened as much as the widest FBG could enable. In the near future, we will investigate the possibility to generate shorter pulses by replacing the current SESAM with a different saturable absorber. The bandwidth limitation could also be caused by free-space propagation required to focus the laser beam on the SESAM due to the reverse design of this SESAM. This would suggest that the water vapor absorption lines seem to be the

ultimate limiting factor to achieve even shorter pulses in this demonstration [35]. With the advent of butt-coupling-enabled mid-IR SAM [33], or a deposited saturable absorber layer on the fiber tip [32], the effect of water vapor absorption lines in the free-space propagation portion of this laser design could be completely eliminated [35]. In addition to making the laser device much more robust and reliable compared to one that combines fiber optics and free-space optics, this would hopefully allow reaching the sub-picosecond pulse width regime. We also demonstrated that the mode-locked pulses are not destabilized when an intracavity pump combiner is included in the design as a preliminary step towards an all-fiber architecture for a mode-locked fiber laser bounded by an FBG and a SESAM.

5. Conclusions

We demonstrate self-starting mode-locked mid-IR fiber lasers based on a broadband uniform FBG and a SESAM that generates pulses as short as 15 ps. The results presented in this report are paving the way towards a mid-IR mode-locked all-fiber laser design. The laser emission spectrum and the pulse duration could be easily adjusted through the FBG bandwidth and peak reflectance as well as the fiber length to suit different applications. Moreover, we demonstrated that a pump combiner could be used in an all-fiber design of such lasers since it does not destabilize the mode-locked pulse train. The ease of pulse adjustments and the potential robustness of an all-fiber design could lead to commercial versions of these mid-IR ultrafast fiber lasers for various applications since they could more easily meet their specific requirements. However, the lack of commercially available butt-coupling-enabled mid-IR SAM is one of the last barriers for the democratization of such lasers to this day.

Future work will focus on a truly all-fiber mid-IR mode-locked fiber laser with the previous components demonstrated in this study to generate shorter pulses and a more robust and reliable ultrafast mid-IR fiber laser. A new SESAM that has a shorter recovery time and that can be butt-coupled to the gain fiber will also be investigated to produce shorter pulses by eliminating the free-space propagation from the design thus avoiding the spectral limitation from the water vapor absorption lines. Field application demonstrations will also be made to ensure the stability and ease of use of these fiber lasers to promote their capabilities.

Author Contributions: Conceptualization, P.P., V.F. and M.B.; methodology, P.P., T.B., V.F. and M.B.; software, P.P.; validation, P.P., R.V. and M.B.; formal analysis, P.P.; investigation, P.P. and T.B.; resources, R.V. and M.B.; data curation, P.P.; writing—original draft preparation, P.P.; writing—review and editing, R.V. and M.B.; visualization, P.P.; supervision, R.V. and M.B.; project administration, R.V. and M.B.; funding acquisition, R.V. and M.B. All authors have read and agreed to the published version of the manuscript.

Funding: The research described herein was sponsored by the Natural Sciences and Engineering Research Council of Canada (CRDPJ-543631-19, IRCPJ469414-18, RGPIN-2016-05877); Canada First Research Excellence Fund (Sentinel North Program); Canada Foundation for Innovation (5180); and the Fonds de recherche du Québec—Nature et technologies (114616, CO256655).

Institutional Review Board Statement: Not applicable.

Informed Consent Statement: Not applicable.

Data Availability Statement: The data presented in this study are available on request from the corresponding author.

Acknowledgments: The authors thank Michel Olivier for fruitful discussions on mode-locking dynamics.

Conflicts of Interest: The authors declare no conflict of interest.

Abbreviations

The following abbreviations are used in this manuscript:

CW	Continuous wave
FBG	Fiber Bragg grating
FROG	Frequency resolved optical gating
FWHM	Full width at half maximum
MCT	Mercury cadmium telluride
Near-IR	Near-infrared
Mid-IR	Mid-infrared
OPA	Optical parametric amplifier
OPO	Optical parametric oscillator
OSA	Optical spectrum analyzer
RF	Radio frequency
SAM	Saturable absorber mirror
SESAM	Semi conductor saturable absorber mirror

References

1. Jackson, S.; Bernier, M.; Vallée, R. (Eds.) *Mid-Infrared Fiber Photonics*, 1st ed.; Woodhead Publishing Series in Electronic and Optical Materials; Elsevier: Sawston, UK, 2021. [\[CrossRef\]](#)
2. Zhu, X.; Zhu, G.; Wei, C.; Kotov, L.V.; Wang, J.; Tong, M.; Norwood, R.A.; Peyghambarian, N. Pulsed fluoride fiber lasers at 3 μm . *J. Opt. Soc. Am. B* **2017**, *34*, 15–28. [\[CrossRef\]](#)
3. Jobin, F.; Paradis, P.; Aydin, Y.O.; Boilard, T.; Fortin, V.; Gauthier, J.C.; Lemieux-Tanguay, M.; Magnan-Saucier, S.; Michaud, L.C.; Mondor, S.; et al. Recent developments in lanthanide-doped mid-infrared fluoride fiber lasers. *Opt. Express* **2022**, *30*, 8615–8640. [\[CrossRef\]](#) [\[PubMed\]](#)
4. Amini-Nik, S.; Kraemer, D.; Cowan, M.L.; Gunaratne, K.; Nadesan, P.; Alman, B.A.; Miller, R.J.D. Ultrafast Mid-IR Laser Scalpel: Protein Signals of the Fundamental Limits to Minimally Invasive Surgery. *PLoS ONE* **2010**, *5*, e13053. [\[CrossRef\]](#) [\[PubMed\]](#)
5. Franjic, K.; Cowan, M.L.; Kraemer, D.; Miller, R.J.D. Laser selective cutting of biological tissues by impulsive heat deposition through ultrafast vibrational excitations. *Opt. Express* **2009**, *17*, 22937–22959. [\[CrossRef\]](#) [\[PubMed\]](#)
6. Jelínková, H. (Ed.) *Lasers for Medical Applications*; Woodhead Publishing: Cambridge, United Kingdom, 2013.
7. Hodgkinson, J.; Tatam, R.P. Optical gas sensing: A review. *Meas. Sci. Technol.* **2013**, *24*, 012004. [\[CrossRef\]](#)
8. Walsh, B.M.; Lee, H.R.; Barnes, N.P. Mid infrared lasers for remote sensing applications. *J. Lumin.* **2016**, *169*, 400–405. [\[CrossRef\]](#)
9. Sorkio, A.; Koch, L.; Koivusalo, L.; Deiwick, A.; Miettinen, S.; Chichkov, B.; Skottman, H. Human stem cell based corneal tissue mimicking structures using laser-assisted 3D bioprinting and functional bioinks. *Biomaterials* **2018**, *171*, 57–71. [\[CrossRef\]](#)
10. Cheng, S.C.; Shiea, C.; Huang, Y.L.; Wang, C.H.; Cho, Y.T.; Shiea, J. Laser-based ambient mass spectrometry. *Anal. Methods* **2017**, *9*, 4924–4935. [\[CrossRef\]](#)
11. Wang, C.; Sahay, P. Breath Analysis Using Laser Spectroscopic Techniques: Breath Biomarkers, Spectral Fingerprints, and Detection Limits. *Sensors* **2009**, *9*, 8230–8262. [\[CrossRef\]](#)
12. Duval, S.; Bernier, M.; Fortin, V.; Genest, J.; Piché, M.; Vallée, R. Femtosecond fiber lasers reach the mid-infrared. *Optica* **2015**, *2*, 623–626. [\[CrossRef\]](#)
13. Hu, T.; Jackson, S.D.; Hudson, D.D. Ultrafast pulses from a mid-infrared fiber laser. *Opt. Lett.* **2015**, *40*, 4226–4228. [\[CrossRef\]](#) [\[PubMed\]](#)
14. Duval, S.; Olivier, M.; Fortin, V.; Bernier, M.; Piché, M.; Vallée, R. 23-kW peak power femtosecond pulses from a mode-locked fiber ring laser at 2.8 μm . *Fiber Lasers XIII Technol. Syst. Appl.* **2016**, *9728*, 972802. [\[CrossRef\]](#)
15. Antipov, S.; Hudson, D.D.; Fuerbach, A.; Jackson, S.D. High-power mid-infrared femtosecond fiber laser in the water vapor transmission window. *Optica* **2016**, *3*, 1373–1376. [\[CrossRef\]](#)
16. Wang, Y.; Jobin, F.; Duval, S.; Fortin, V.; Laporta, P.; Bernier, M.; Galzerano, G.; Vallée, R. Ultrafast Dy³⁺:fluoride fiber laser beyond 3 μm . *Opt. Lett.* **2019**, *44*, 395–398. [\[CrossRef\]](#)
17. Bawden, N.; Henderson-Sapir, O.; Jackson, S.D.; Ottaway, D.J. Ultrafast 3.5 μm fiber laser. *Opt. Lett.* **2021**, *46*, 1636–1639. [\[CrossRef\]](#)
18. Huang, J.; Pang, M.; Jiang, X.; Köttig, F.; Schade, D.; He, W.; Butryn, M.; Russell, P.S.J. Sub-two-cycle octave-spanning mid-infrared fiber laser. *Optica* **2020**, *7*, 574–579. [\[CrossRef\]](#)
19. Zhou, Y.; Qin, Z.; Yuan, P.; Ma, J.; Xie, G. 2-MW peak-power pulses from a dispersion-managed fluoride fiber amplifier at 2.8 μm . *Opt. Lett.* **2021**, *46*, 5104–5107. [\[CrossRef\]](#) [\[PubMed\]](#)
20. Tang, P.; Qin, Z.; Liu, J.; Zhao, C.; Xie, G.; Wen, S.; Qian, L. Watt-level passively mode-locked Er³⁺-doped ZBLAN fiber laser at 2.8 μm . *Opt. Lett.* **2015**, *40*, 4855–4858. [\[CrossRef\]](#)
21. Wei, C.; Zhu, X.; Norwood, R.A.; Peyghambarian, N. Passively continuous-wave mode-locked Er³⁺-doped ZBLAN fiber laser at 2.8 μm . *Opt. Lett.* **2012**, *37*, 3849–3851. [\[CrossRef\]](#)

22. Qin, Z.; Xie, G.; Zhao, C.; Wen, S.; Yuan, P.; Qian, L. Mid-infrared mode-locked pulse generation with multilayer black phosphorus as saturable absorber. *Opt. Lett.* **2016**, *41*, 56–59. [[CrossRef](#)]
23. Zhu, F.; Bicer, A.; Askar, R.; Bounds, J.; Kolomenskii, A.A.; Kelessides, V.; Amani, M.; Schuessler, H.A. Mid-infrared dual frequency comb spectroscopy based on fiber lasers for the detection of methane in ambient air. *Laser Phys. Lett.* **2015**, *12*, 095701. [[CrossRef](#)]
24. Luo, H.; Wang, Y.; Li, J.; Liu, Y. High-stability, linearly polarized mode-locking generation from a polarization-maintaining fiber oscillator around 2.8 μm . *Opt. Lett.* **2021**, *46*, 4550–4553. [[CrossRef](#)]
25. Luo, H.; Li, S.; Wu, X.; Kang, Z.; Li, J.; Qin, G.; Qin, W.; Liu, Y. Unlocking the ultrafast potential of gold nanowires for mode-locking in the mid-infrared region. *Opt. Lett.* **2021**, *46*, 1562–1565. [[CrossRef](#)] [[PubMed](#)]
26. Li, J.; Hudson, D.D.; Liu, Y.; Jackson, S.D. Efficient 2.87 μm fiber laser passively switched using a semiconductor saturable absorber mirror. *Opt. Lett.* **2012**, *37*, 3747–3749. [[CrossRef](#)] [[PubMed](#)]
27. Hu, T.; Hudson, D.D.; Jackson, S.D. Stable, self-starting, passively mode-locked fiber ring laser of the 3 μm class. *Opt. Lett.* **2014**, *39*, 2133–2136. [[CrossRef](#)] [[PubMed](#)]
28. Yin, K.; Jiang, T.; Zheng, X.; Yu, H.; Cheng, X.; Hou, J. Mid-infrared ultra-short mode-locked fiber laser utilizing topological insulator Bi_2Te_3 nano-sheets as the saturable absorber. *arXiv* **2015**, arXiv:1505.06322. <https://doi.org/10.48550/arXiv.1505.06322>.
29. Qin, Z.; Hai, T.; Xie, G.; Ma, J.; Yuan, P.; Qian, L.; Li, L.; Zhao, L.; Shen, D. Black phosphorus Q-switched and mode-locked mid-infrared Er:ZBLAN fiber laser at 3.5 μm wavelength. *Opt. Express* **2018**, *26*, 8224–8231. [[CrossRef](#)]
30. Qin, Z.; Chai, X.; Xie, G.; Xu, Z.; Zhou, Y.; Wu, Q.; Li, J.; Wang, Z.; Weng, Y.; Hai, T.; et al. Semiconductor saturable absorber mirror in the 3–5 μm mid-infrared region. *Opt. Lett.* **2022**, *47*, 890–893. [[CrossRef](#)]
31. Haboucha, A.; Fortin, V.; Bernier, M.; Genest, J.; Messaddeq, Y.; Vallée, R. Fiber Bragg grating stabilization of a passively mode-locked 2.8 μm Er^{3+} : Fluoride glass fiber laser. *Opt. Lett.* **2014**, *39*, 3294–3297. [[CrossRef](#)]
32. Qin, Z.; Xie, G.; Ma, J.; Yuan, P.; Qian, L. 2.8 μm all-fiber Q-switched and mode-locked lasers with black phosphorus. *Photonics Res.* **2018**, *6*, 1074–1078. [[CrossRef](#)]
33. Bharathan, G.; Xu, L.; Jiang, X.; Zhang, H.; Li, Z.; Chen, F.; Fuerbach, A. MXene and PtSe_2 saturable absorbers for all-fibre ultrafast mid-infrared lasers. *Opt. Mater. Express* **2021**, *11*, 1898–1906. [[CrossRef](#)]
34. Bernier, M.; Trepanier, F.; Carrier, J.; Vallée, R. Efficient writing of Bragg gratings through the coating of various optical fibers. In *Bragg Gratings, Photosensitivity, and Poling in Glass Waveguides*; Optica Publishing Group: Washington, DC, USA, 2014; p. BM2D.3. [[CrossRef](#)]
35. Majewski, M.R.; Pawlizewska, M.; Jackson, S.D. Picosecond pulse formation in the presence of atmospheric absorption. *Opt. Express* **2021**, *29*, 19159–19169. [[CrossRef](#)] [[PubMed](#)]
36. Paradis, P.; Duval, S.; Fortin, V.; Vallée, R.; Bernier, M. Towards Ultrafast All-Fiber Laser at 2.8 μm Based on a SESAM and a Fiber Bragg Grating. In Proceedings of the 2019 Conference on Lasers and Electro-Optics Europe and European Quantum Electronics Conference, Munich, Germany, 23–27 June 2019; p. 1. [[CrossRef](#)]
37. Richardson, D.J.; Nilsson, J.; Clarkson, W.A. High power fiber lasers: Current status and future perspectives. *J. Opt. Soc. Am. B* **2010**, *27*, B63. [[CrossRef](#)]
38. Abas, A.F.; Lau, K.Y.; Abdulkawi, W.M.; Alresheedi, M.T.; Muhammad, F.D.; Mahdi, M.A. Dispersion Management and Pulse Characterization of Graphene-Based Soliton Mode-Locked Fiber Lasers. *Appl. Sci.* **2022**, *12*, 3288. [[CrossRef](#)]

Disclaimer/Publisher’s Note: The statements, opinions and data contained in all publications are solely those of the individual author(s) and contributor(s) and not of MDPI and/or the editor(s). MDPI and/or the editor(s) disclaim responsibility for any injury to people or property resulting from any ideas, methods, instructions or products referred to in the content.